Rapid Communications

Direct observation of ultracold atom-ion excitation exchange

Ruti Ben-shlomi,[1,*] Romain Vexiau,[2] Ziv Meir,[1,†] Tomas Sikorsky,[1,‡] Nitzan Akerman,[1] Meirav Pinkas,[1] Olivier Dulieu,[2] and Roee Ozeri[1]

[1]*Department of Physics of Complex Systems, Weizmann Institute of Science, Rehovot 7610001, Israel*

[2]*Laboratoire Aimé Cotton, CNRS/Université Paris-Sud/ENS Paris-Saclay/Université Paris-Saclay, Orsay Cedex, France*

(Received 17 September 2019; revised 19 August 2020; accepted 19 August 2020; published 16 September 2020)

Ultracold atom-ion collisions are an emerging field of research that can ultimately lead to their precise quantum control. In collisions in which the ion is prepared in an excited state, previous studies showed that the dominant reaction pathway was charge exchange. Here, we explored the outcome products and the energy released from a single ultracold collision between a single $^{88}Sr^{+}$ ion and a single ^{87}Rb atom prepared in excited metastable and ground electronic states, respectively, with control over their relative spins. We found that the ion's long-lived $D_{5/2}$ and $D_{3/2}$ states quench after roughly three collisions, acquiring immense kinetic energy in the process. By performing single-shot thermometry on the ion after the collision, we identified two dominant reaction pathways: electronic excitation exchange and spin-orbit change. In contrast to previous experiments, we observed no charge-exchange events. These processes are theoretically understood to occur through Landau-Zener avoided crossings leading to the observed reaction pathways. We also found that spin orientation has almost no effect on the reaction pathways, due to strong Coriolis-spin mixing. Our results provide a deeper understanding of ultracold atom-ion inelastic collisions and offer additional quantum control tools for the cold chemistry field.

DOI: 10.1103/PhysRevA.102.031301

One of the most challenging contemporary goals in the research of cold atoms is to study a single ultracold collision and gain full quantum control over its outcomes and reaction pathways [1–7]. Ultracold atom-ion systems offer excellent tools to investigate such cold inelastic collisions. The high fidelity with which trapped ions and atoms can be coherently controlled enables their preparation in well-defined internal and motional states prior to the collision. Similarly, the state of ions and atoms following the collision can be analyzed with great precision. Several collisional processes have been recently studied in ultracold atom-ion mixtures. Examples include charge-exchange reactions between atoms and ions [7–15], atoms and molecular ions [16], and Rydberg atoms and ions [17]. More reaction pathways include spin exchange and spin relaxation [18–22], molecular formation [12,23–25], as well as three-body recombination [26,27].

Some of the experiments mentioned above were carried out with both the atom and ion prepared in their electronic ground state. However, if one of the colliding partners is prepared in an excited electronic state, more inelastic channels become available, leading to richer dynamics, but also to various challenges in the theoretical interpretation. Inelastic atom-ion collisions with the ion prepared in an optically excited metastable state were recently studied [7,8,11,28]. These metastable states of ions are important since they serve as excited states in optical frequency standards [29] and quantum computing [30] applications. In previous experiments, the lifetime of these excited states and the ionic outcome products of such collisions were measured. However, the lack of ability to measure the energy of the outgoing collision products prevented detailed experimental identification of the underlying mechanisms.

Here we report on the observation of the quick relaxation of the long-lived $4d\,^2D_{3/2,5/2}$ (hereafter referred to as the $D_{3/2}$ and $D_{5/2}$ states, for simplicity), atomic levels of $^{88}Sr^{+}$ when colliding with ultracold ^{87}Rb atoms in the ground state. We found that the $^{88}Sr^{+}$ ion quickly quenches from the $D_{5/2}$ and $D_{3/2}$ states, after three collisions on average. Exploiting a newly developed single-shot Doppler cooling thermometry (SSDCT) [31], we measured the distribution of the kinetic energies of the ion after the quench. The measured energy distribution of the ionic product allowed us to identify two relaxation processes: electronic excitation exchange (EEE) and spin-orbit change (SOC). Using accurate molecular structure calculations we showed that these processes are induced by short-range interactions, manifested by avoided crossings of the corresponding potential energy curves (PECs) of the $RbSr^{+}$ molecule. The SOC channel can be turned on or off by initializing the ion in the $D_{5/2}$ or $D_{3/2}$ level, respectively.

We investigated these cold collisions when the ion and atoms are polarized in different spin states. To the best of our knowledge, this is the first study of spin-polarized atom-ion collisions where the ion is in a metastable excited state. We found that the initial mutual spin orientation of the atom and ion has almost no effect on these processes, indicating a high

*ruti.ben-shlomi@weizmann.ac.il

†Present address: Department of Chemistry, University of Basel, Klingelbergstrasse 80, CH-4056 Basel, Switzerland.

‡Present address: Atominstitut-E141, Technische Universität Wien, Stadionallee 2, 1020 Vienna, Austria.

degree of angular momentum mixing during the collision. With our typical atom-ion center-of-mass kinetic energy of 0.5 mK $\times$ k_B, up to ~20 partial waves participate in the collision. This high rotational motion generates strong Coriolis forces which are responsible for this angular momentum mixing. This finding is in contrast to a previous study [20], where spin-aligned atom-ion configuration was found to be protected from inelastic reactions. As opposed to this previous work where the ion collided with the atoms at its electronic ground state, here, the ion is excited to the $D_{5/2}$ state. This leads to more molecular symmetries and available angular momentum due to the excitation, thus more possibilities to couple.

Surprisingly, we did not observe enhanced charge-exchange reaction rates when the ion was initialized in one of the excited D states. The measured upper bound on the probability of undergoing a charge-exchange reaction during a collision when the ion is in this excited state is $P < 1 \times 10^{-4}$. This is in contrast to all previous observations in which charge-exchange reaction pathways dominated collisions in which atoms or ions were in excited states [7,8,11–14,16,17,24,28]. Here, charge exchange was not observed, despite being energetically allowed, since the collision entrance channel has no avoided crossings with $Rb^+ + Sr$ PECs which are located below the dissociation energy, and therefore do not couple [see Fig. 1(a) of the Supplemental Material [32]). Charge-exchange events are usually undesirable since they involve ion loss and thus have been a limiting factor in atom-ion research.

In our experiment, ~20 000 ultracold (3 μK) ^{87}Rb atoms are trapped in an optical dipole trap (ODT) and overlapped with a single cold (40 μK) $^{88}Sr^+$ ion which is trapped in a linear rf Paul trap [33]. Combination of imperfect micromotion compensation and a fundamental limit for achievable atom-ion collision energy in Paul traps [34,35] set the typical center-of-mass energy, during the first few collisions, to be roughly 0.5 mK $\times$ k_B. We initially prepared the ion in one of the internal, metastable, excited $D_{5/2}$ or $D_{3/2}$ levels (with natural lifetimes of 390 and 435 ms, respectively) and the atoms in the $S_{1/2}$ ground state. We overlapped the cloud of atoms with the single trapped ion for different interaction times, allowing one to few Langevin collisions on average, with a typical Langevin collision rate of 0.5 kHz (see Supplemental Material Secs. I and II for details). After the interaction, the atoms were released from the trap and were measured by absorption imaging after a short time of flight. Finally, the ion state and kinetic energy were interrogated using a 422-nm laser close to resonance with its $5s\,^2S_{1/2}$-$4p\,^2P_{1/2}$ dipole-allowed transition (or $S_{1/2}$-$P_{1/2}$ in short; see Supplemental Material Sec. I). All experiments were repeated with an interlaced comparison without the presence of atoms.

In a first experiment, we measured the probability that the ion remains in the metastable D level as a function of the interaction time. Figure 1(a) shows this probability in the case where the ion was initialized in the $m_{J_e} = -5/2$ Zeeman sublevel of the $D_{5/2}$ manifold using electron shelving with a narrow linewidth laser (lower, blue data points), and in the case where the ion was initialized in the $D_{3/2}$ level with unpolarized spin using optical pumping on the strong $S_{1/2}$-$P_{1/2}$ dipole-allowed transition (upper, red data points). In both cases the atoms were prepared

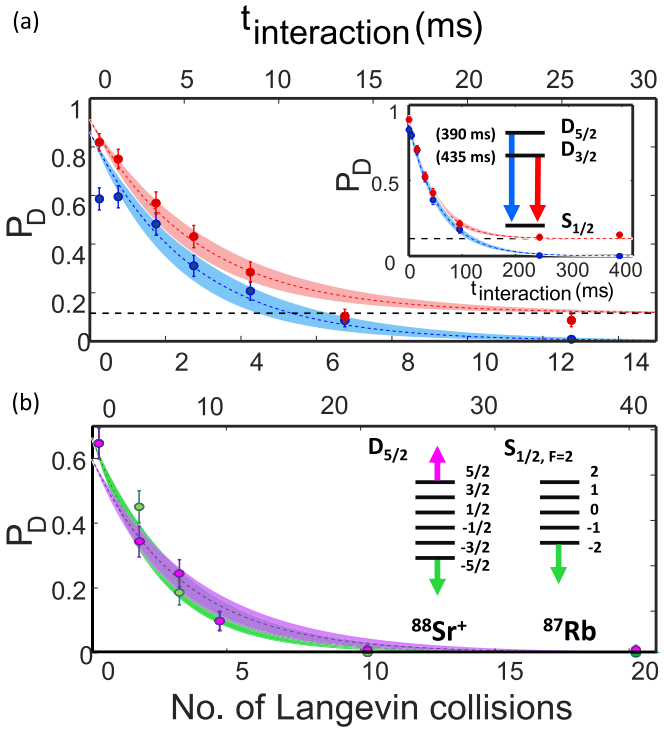

FIG. 1. Decay of the ion population from the metastable $D_{3/2,5/2}$ states. (a) Population decay from the $D_{5/2}$ (lower, blue curve) and $D_{3/2}$ (upper, red curve) states in the absence (inset) and in the presence of atoms. Error bars correspond to one σ standard deviation. The natural lifetimes of these levels are 390 and 435 ms, correspondingly. The fitted dashed curves are the solutions to rate equations yielding exponential decay. The shaded areas represent exponential-fit confidence bounds of one σ on the decay rate. Population is seen to decay after $\simeq$3 Langevin collisions on average. (b) Population decay from the $D_{5/2}$ level, when ^{87}Rb atoms are polarized in the $m_F = -2$ hyperfine Zeeman state, and the ion is polarized to the $m_{J_e} = -5/2$ state, as indicated by the green (light-gray) curve, or the $m_{J_e} = +5/2$ state, as indicated by the purple (dark-gray) curve. These two configurations correspond to the atom and ion internal angular momentum being parallel vs antiparallel.

in the $F = 1$ hyperfine manifold of their $S_{1/2}$ ground state without any preferred spin polarization. When the ion was initialized in the $D_{3/2}$ level the probability did not asymptotically approach zero due to an artifact in our $D_{3/2}$ level population measurement (see Supplemental Material Sec. II for details). The collisional quenching rate Γ_Q is extracted from a fit to the solution of a rate equation, shown by the dashed lines (see Supplemental Material Sec. II). Here, the rate at which both D levels decay in the absence of atoms, due to off-resonance scattering of photons from the ODT laser beam at 1064 nm, had to be taken into account. This rate was calibrated in a separate measurement shown in the inset of Fig. 1(a). The extracted rates at which the two levels decayed from the $D_{5/2}$ and $D_{3/2}$ states are $\Gamma_Q = 2.6(4)$ and $\Gamma_Q = 2.8(3)$ Langevin collisions on average, respectively.

Events in which the ion decayed from the D level were identified either by state-selective fluorescence, indicating that the ion is cold and in the $S_{1/2}$ ground state, or by observing that the ion has heated up significantly and no fluorescence

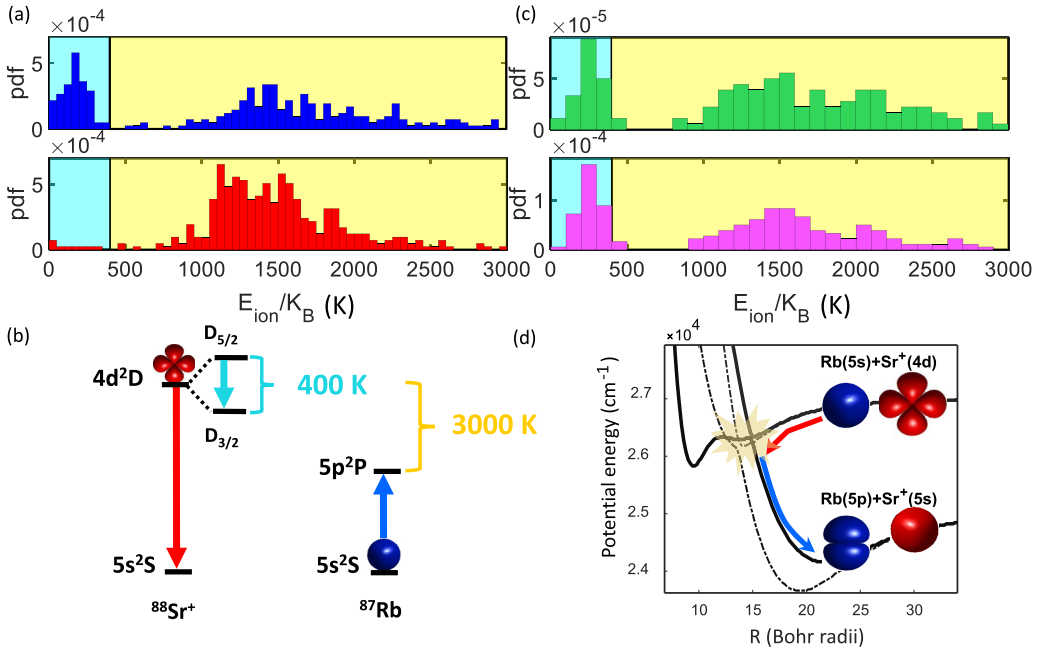

FIG. 2. Histograms of the energy released in quench events. (a) Quenching events from the $D_{5/2}$ (top) and $D_{3/2}$ states (bottom). Both exhibit a broad energy distribution around 1500 K $\times\, k_B$, corresponding to the EEE channel (marked by the right, yellow background). The $D_{5/2}$ histogram displays a second peak around 200 K $\times\, k_B$, corresponding to the SOC channel (marked by the left, cyan background). The collision probability for this experiment is low, therefore a few events at temperatures lower than 500 K for the $D_{3/2}$ case are likely the result of sympathetic cooling. (b) Relevant energy levels of $^{88}Sr^+$ and ^{87}Rb. The $4d\,^2D$ level in Sr^+ splits into two spin-orbit components separated by ∼400 K $\times\, k_B$, which are coupled by the SOC channel (short, cyan down arrow). The energy difference of the EEE channel (long, red down arrow and blue upper arrow) is ∼3000 K $\times\, k_B$. (c) Quenching events from the $D_{5/2}$ state, when the internal angular momentum states of $^{88}Sr^+$ and ^{87}Rb are prepared in an aligned (top green, referred to as $\downarrow_i\downarrow_a$) and antialigned (bottom purple, referred to as $\uparrow_i\downarrow_a$) configuration [see Fig. 1(b)]. The ratios between the corresponding rates are $\Gamma_{\rm SO}^{\downarrow_i\downarrow_a}/\Gamma_{\rm EEE}^{\downarrow_i\downarrow_a} = 31(4)\%$ and $\Gamma_{\rm SO}^{\uparrow_i\downarrow_a}/\Gamma_{\rm EEE}^{\uparrow_i\downarrow_a} = 47(7)\%$. (d) Schematic illustration of the quenching process leading to EEE, and of the relevant $(RbSr)^+$ molecular PECs presented in Hund's case *a* form. The process is induced by a localized avoided crossing between two curves [solid: $^1\Sigma^+$; dashed: $^3\Sigma^+$; see also Fig. 1(b) in the Supplemental Material], leading to a large kinetic energy release of ∼3000 K $\times\, k_B$ distributed equally between the atomic and ionic products.

is recorded even after optically pumping the ion to the $S_{1/2}$ ground state due to very large Doppler shifts (see Supplemental Material Sec. I). By comparing the measured collisional quench rate to the rate at which hot ion events were recorded, we concluded that the ion considerably heated up every time it collisionally quenched from the D level, indicating that the quench is nonradiative and releases the internal electronic energy difference into atomic motion.

We next turned to investigate the dependence of the quench rate on the mutual spin orientation of the ion and atom. We interlaced the experiment between initializing the ion in the $D_{5/2},\ m_{J_e} = -5/2$ and the $D_{5/2},\ m_{J_e} = +5/2$ spin states. The atoms were prepared in the stretched spin state $F = 2,\ m_{\rm F} = -2$. Here, when the ion and atom spins are aligned, the total electronic angular momentum of the atom-ion complex is $3\hbar$. Since there is no lower electronic energy level that carries that much angular momentum, a nonradiative decay would imply the transfer of angular momentum from the electronic degrees of freedom to rotation of nuclei. Such coupling between internal and rotation angular momenta in ultracold collisions is usually weak [36], so that we would expect the parallel-spin quench rate to be suppressed as compared with the antiparallel spin case. Figure 1(b) shows the two measured decay curves. Using a fit to the measured data we found that the ion quenches from the $D_{5/2}$ level after $\Gamma_Q = 2.4(2)$ $(m_{J_e} = -5/2)$ and $\Gamma_Q = 3.0(3)$ $(m_{J_e} = 5/2)$ Langevin collisions on average. Strikingly, the quenching rates for the parallel-spin orientation is not substantially suppressed compared to the antiparallel case, indicating strong electronic angular momentum transfer to molecular rotation.

To better understand the reaction pathways of the quench, we investigated the spectrum of the released kinetic energies using SSDCT on the ion (see Supplemental Material Sec. III and Refs. [31,37]). With SSDCT, we measured the ionic product kinetic energy in a single shot, i.e., for every experimental repetition independently, provided that this energy is above $\simeq$ 10 K $\times\, k_B$. Here we set the interaction time to be sufficiently short (∼0.5 ms), to avoid multiple elastic collisions leading to sympathetic cooling of the ion after the quench event.

The upper histogram in Fig. 2(a) shows the distribution of energies measured following a quench of the $D_{5/2}$ level. Two clear separate energy distributions emerge with one peak around $\simeq$200 K $\times\, k_B$ and another around $\simeq$1500 K $\times\, k_B$. These energies can easily be associated with decay channels by considering the energy differences between atomic levels shown in Fig. 2(b). Decay from the entrance channel $\mathrm{Rb}(S_{1/2}) + \mathrm{Sr}^+(D_{5/2})$ to the $\mathrm{Rb}(P_{1/2,3/2}) + \mathrm{Sr}^+(S_{1/2})$ channels (EEE channels), releases a kinetic energy of $\simeq$3230 K $\times\, k_B$ and $\simeq$ 2890 K $\times\, k_B$, respectively. This energy is almost equally divided between ^{87}Rb and $^{88}Sr^+$ owing to their nearly

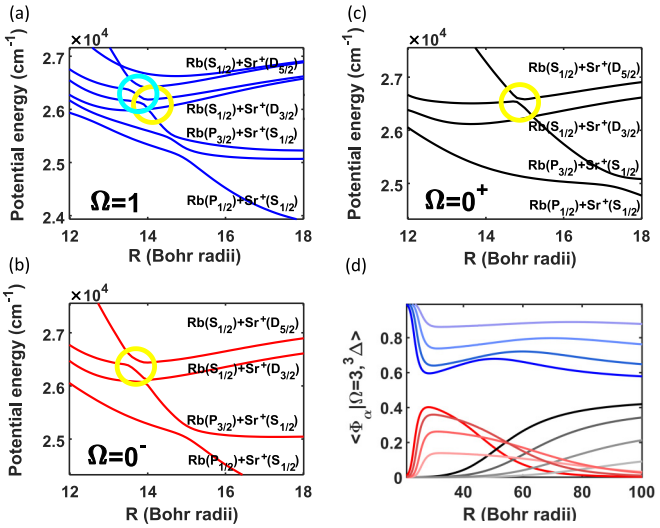

FIG. 3. Potential energy curves for the excited states including spin-orbit interaction. (a),(b),(c) RbSr$^+$ PECs in Hund's case *c* representation, including SO interaction for the two displayed asymptotes (see text). The symmetries $\Omega = 1, 0^{\pm}$ are displayed as blue, red, and black lines in different frames for clarity [in (a), (b), and (c), respectively). The avoided crossings for the SOC and EEE processes are marked with cyan (dark-gray) and three yellow (light-gray) circles, respectively. (d) The component on the $\Omega = 3$, ($^3\Delta$) Hund's case *c* state of three of the eigenvectors Φ_α (top blue, bottom-left red, and bottom-right black curves) of the full Hamiltonian matrix including SO and Coriolis couplings (see Supplemental Material Sec. V). Each is also plotted for four values of the maximal angular momentum, $J = 3, 5, 10, 20$ (from bright to dark color, respectively).

equal masses, resulting in the peak around $\simeq$1500 K $\times\, k_B$. Similarly, a quench to the Rb$(S_{1/2}) + \mathrm{Sr}^+(D_{3/2})$ channel (SOC channel), releases of $\simeq$402 K $\times\, k_B$, resulting in the peak around $\simeq$200 K $\times\, k_B$.

A similar analysis of the energies measured using SSDCT when the ion is initialized in the $D_{3/2}$ state is shown by the lower red histogram in Fig. 2(a). As seen here, only the $\simeq$ 1500 K $\times\, k_B$ EEE channel remains. The SOC channel cannot be endothermically excited at such a low initial temperature. Therefore, the SOC channel can be turned on or off by initializing the ion in the $D_{5/2}$ or $D_{3/2}$ level.

Finally, we compared the spectrum of energies released between the cases where the electronic spins of the ion and atoms are aligned parallel or antiparallel [same levels as those used in Fig. 1(b)]. The two spectra are shown in Fig. 2(c). As seen, no significant difference can be observed between the two cases, again suggesting strong angular momentum mixing.

We now turn to a theoretical analysis of the quench process. Figure 2(d) provides a schematic illustration of the dynamics we observed. When the ground state Rb atom and the excited Sr^+ ion approach each other their electronic wave functions are strongly perturbed by their interaction, leading to avoided crossings between molecular potential curves. Nonadiabatic transitions through these crossings leads to the large release of kinetic energy.

In order to explain the SOC channel, we present in Fig. 3 the numerically calculated RbSr$^+$ PECs varied over the internuclear distance R, including spin-orbit (SO) coupling. As the molecular R-dependent SO coupling is unknown, we rely on an asymptotic model involving the atomic SO splittings [38–40]. Here, we observed avoided crossings in three of the resulting symmetries $\Omega = 0^{\pm}, 1$, where Ω is the projection of the total electronic angular momentum on the molecular axis. No avoided crossing occurs in the $\Omega = 2, 3$ symmetries. We identified EEE (SOC) transitions through three (one) avoided crossings marked by yellow (cyan) circles. We analyzed the expected transition probabilities through these avoided crossings using a multicrossing Landau-Zener model (all calculated and measured transition probabilities are compared in Table I in Supplemental Material Sec. IV).

We found that while qualitatively producing the EEE and SOC channels, our experimentally measured probabilities are higher than the predictions of the model. This disagreement persists even when considering the maximal transition probability case. Furthermore, as shown above, even when preparing the atom-ion complex with total angular momentum $3\hbar$, the quenching probability remains high, while this calculation confirms that conservation of internal angular momentum implies complete protection against nonadiabatic quench. Both these observations suggest significant coupling between the Hunds case *c* PECs and transfer of internal electronic angular momentum to molecular rotation through inertial coupling.

Typically, in ultracold collisions, such inertial coupling is small due to the small number of partial waves involved. However, in atom-ion collisions the number of partial waves can be large even in the few hundreds of $\mu\mathrm{K} \times k_B$ energy range, due to the relatively long-ranged R^{-4} atom-ion interaction. In our experiment up to 20 partial waves contribute in the collision, and therefore molecular rotation may be strongly coupled to internal electronic angular momentum. This results in coupling between the PECs in Fig. 3 and therefore the hypothesis of population distributed statistically across all PECs, used in deriving the theoretical probabilities, is compromised.

To show the effect of inertial coupling, we add a rotational term to the SO matrices (see Supplemental Material Sec. VI). Strong angular momentum mixing is confirmed by the results of Fig. 3(d). In the molecular structure calculations, the fully aligned situation is correlated to the molecular state with the highest angular momentum, namely, the $\Omega = 3$ Hund's case *c* state, composed solely from the $^3\Delta$ Hund's case *a* state. This symmetry does not exhibit any avoided crossing, so that it must be strongly mixed with other molecular states to undergo quenching. As an illustration, Fig. 3(d) displays the component on the $\Omega = 3$, ($^3\Delta$) Hund's case *c* state of three of the eigenvectors Φ_α of the full Hamiltonian matrix including SOC and Coriolis coupling. These plots demonstrate that the $\Omega = 3$, ($^3\Delta$) is indeed strongly coupled to other states at infinity, and the coupling increases with J. Even in the case of *s*-wave collision, where $J = 3$, there still exists a degree of angular mixing, indicating that this fully aligned state lacks protection even at very low temperatures. As opposed to atom-ion collisions in which the two parties are in the electronic ground state, collisions in electronic excited states involve strong angular mixing which compel the lack of protection of the protected triplet state $^3\Delta$.

To conclude, we have studied the dynamics of an ion, initialized in a metastable excited electronic level, during collisions with ultracold atoms in their electronic ground state. By measuring the final kinetic energy of the ion after a single collision we found that two nonadiabatic quench processes occur. The first is an excitation exchange between the atom and ion and the second is a change of the fine-structure level of the ion excited state. These nonradiative decay channels happen through avoided crossings, releasing the remaining internal energy into molecular motion. Comparing our results with molecular structure calculations suggests that due to the high partial waves involved in this collision and the presence of high internal angular momentum, the electronic angular momentum is mixed through Coriolis coupling, leading to the transfer of electronic angular momentum to external nuclei rotation. Furthermore, this strong angular momentum mixing causes the lack of protection of the fully aligned internal state in the laboratory frame. We also found that due to the lack of avoided crossings with $Rb^+ + Sr$ underlying PECs, we did not observe charge-exchange reaction which is the dominant inelastic reaction pathway in atom-ion mixtures. Our findings shed light on the dynamics of inelastic atom-ion collisions and pave the way for controlling cold chemical reactions at a single collision level.

This work was supported by the Crown Photonics Center, the Israeli Science Foundation, the Israeli Ministry of Science Technology and Space, and the European Research Council (Cconsolidator Grant No. 616919-Ionology).

[1] L. A. Reynolds, E. Schwartz, U. Ebling, M. Weyland, J. Brand, and M. F. Andersen, Phys. Rev. Lett **124**, 073401 (2020).
[2] A. Klein, Y. Shagam, W. Skomorowski, P. S. Żuchowski, M. Pawlak, L. M. C. Janssen, N. Moiseyev, S. Y. T. van de Meerakker, A. van der Avoird, C. P. Koch, and E. Narevicius, Nat. Phys. **13**, 35 (2016).
[3] A. S. Flores, W. Vassen, and S. Knoop, Phys. Rev. A **94**, 050701(R) (2016).
[4] P. Puri, M. Mills, C. Schneider, I. Simbotin, J. A. Montgomery, Jr., R. Côté, A. G. Suits, and E. R. Hudson, Science **357**, 1370 (2017).
[5] M.-G. Hu, Y. Liu, D. D. Grimes, Y.-W. Lin, A. H. Gheorghe, R. Vexiau, N. Bouloufa-Maafa, O. Dulieu, T. Rosenband, and K.-K. Ni, Science **366**, 1111 (2019).
[6] M.-G. Hu, Y. Liu, M. A. Nichols, L. Zhu, G. Quéméner, O. Dulieu, and K.-K. Ni, arXiv:2005.10820.
[7] L. Ratschbacher, C. Zipkes, C. Sias, and M. Köhl, Nat. Phys. **8**, 649 (2012).
[8] S. Haze, R. Saito, M. Fujinaga, and T. Mukaiyama, Phys. Rev. A **91**, 032709 (2015).
[9] M. Tacconi, F. A. Gianturco, and A. K. Belyaev, Phys. Chem. Chem. Phys. **13**, 19156 (2011).
[10] S. Dutta and S. A. Rangwala, Phys. Rev. A **97**, 041401(R) (2018).
[11] J. Joger, H. Fürst, N. Ewald, T. Feldker, M. Tomza, and R. Gerritsma, Phys. Rev. A **96**, 030703(R) (2017).
[12] F. H. J. Hall, M. Aymar, N. Bouloufa-Maafa, O. Dulieu, and S. Willitsch, Phys. Rev. Lett. **107**, 243202 (2011).
[13] W. G. Rellergert, S. T. Sullivan, S. Kotochigova, A. Petrov, K. Chen, S. J. Schowalter, and E. R. Hudson, Phys. Rev. Lett. **107**, 243201 (2011).
[14] A. T. Grier, M. Cetina, F. Orusevic, and V. Vuletic, Phys. Rev. Lett. **102**, 223201 (2009).
[15] S. Schmid, A. Härter, and J. H. Denschlag, Phys. Rev. Lett. **105**, 133202 (2010).
[16] A. D. Dörfler, P. Eberle, D. Koner, M. Tomza, M. Meuwly, and S. Willitsch, Nat. Commun. **10**, 5429 (2019).
[17] N. V. Ewald, T. Feldker, H. Hirzler, H. A. Fürst, and R. Gerritsma, Phys. Rev. Lett **122**, 253401 (2019).
[18] L. Ratschbacher, C. Sias, L. Carcagni, J. M. Silver, C. Zipkes, and M. Köhl, Phys. Rev. Lett. **110**, 160402 (2013).
[19] T. Sikorsky, M. Morita, Z. Meir, A. A. Buchachenko, R. Ben-shlomi, N. Akerman, E. Narevicius, T. V. Tscherbul, and R. Ozeri, Phys. Rev. Lett. **121**, 173402 (2018).
[20] T. Sikorsky, Z. Meir, R. Ben-shlomi, N. Akerman, and R. Ozeri, Nat. Commun. **9**, 920 (2018).
[21] H. Fürst, T. Feldker, N. V. Ewald, J. Joger, M. Tomza, and R. Gerritsma, Phys. Rev. A **98**, 012713 (2018).
[22] T. V. Tscherbul, P. Brumer, and A. A. Buchachenko, Phys. Rev. Lett. **117**, 143201 (2016).
[23] H. da Silva, Jr., M. Raoult, M. Aymar, and O. Dulieu, New J. Phys. **17**, 045015 (2015).
[24] F. H. J. Hall, P. Eberle, G. Hegi, M. Raoult, M. Aymar, O. Dulieu, and S. Willitsch, Mol. Phys. **111**, 2020 (2013).
[25] F. H. J. Hall, M. Aymar, M. Raoult, O. Dulieu, and S. Willitsch, Mol. Phys. **111**, 1683 (2013).
[26] A. Härter, A. Krükow, A. Brunner, W. Schnitzler, S. Schmid, and J. H. Denschlag, Phys. Rev. Lett **109**, 123201 (2012).
[27] A. Mohammadi, A. Krükow, A. Mahdian, M. Deiß, J. Pérez-Ríos, H. da Silva, Jr., M. Raoult, O. Dulieu, and J. H. Denschlag, arXiv:2005.09338.
[28] R. Saito, S. Haze, M. Sasakawa, R. Nakai, M. Raoult, H. Da Silva, Jr., O. Dulieu, and T. Mukaiyama, Phys. Rev. A **95**, 032709 (2017).
[29] H. S. Margolis, G. P. Barwood, G. Huang, H. A. Klein, S. N. Lea, K. Szymaniec, and P. Gil, Science **306**, 1355 (2004).
[30] F. Schmidt-Kaler, S. Gulde, M. Riebe, T. Deuschle, A. Kreuter, G. Lancaster, C. Becher, J. Eschner, H. Häffner, and R. Blatt, J. Phys. B: At., Mol. Opt. Phys. **36**, 623 (2003).
[31] Z. Meir, T. Sikorsky, N. Akerman, R. Ben-shlomi, M. Pinkas, and R. Ozeri, Phys. Rev. A **96**, 020701(R) (2017).
[32] See Supplemental Material at http://link.aps.org/supplemental/10.1103/PhysRevA.102.031301 for detailed description of the experimental measurements, single-shot Doppler cooling thermometry method and rate equation. A detailed theoretical explanation on the calculated Landau-Zener probabilities, and a detailed description on the spin-orbit and Coriolis couplings carried out to explain the data in the text.
[33] Z. Meir, T. Sikorsky, R. Ben-shlomi, N. Akerman, M. Pinkas, Y. Dallal, and R. Ozeri, J. Mod. Opt. **65**, 501 (2018).
[34] M. Cetina, A. T. Grier, and V. Vuletić, Phys. Rev. Lett. **109**, 253201 (2012).

[35] Z. Meir, T. Sikorsky, R. Ben-shlomi, N. Akerman, Y. Dallal, and R. Ozeri, Phys. Rev. Lett. **117**, 243401 (2016).

[36] F. H. Mies, C. J. Williams, P. S. Julienne, and M. Krauss, J. Res. Natl. Inst. Technol. **101**, 521 (1996).

[37] Z. Meir, M. Pinkas, T. Sikorsky, R. Ben-shlomi, N. Akerman, and R. Ozeri, Phys. Rev. Lett. **121**, 053402 (2018).

[38] M. Aymar, R. Guérout, and O. Dulieu, J. Chem. Phys. **135**, 064305 (2011).

[39] R. Beuc, M. Movre, V. Horvatic, C. Vadla, O. Dulieu, and M. Aymar, Phys. Rev. A **75**, 032512 (2007).

[40] J. Lozeille, A. Fioretti, C. Gabbanini, Y. Huang, H. K. Pechkis, D. Wang, P. L. Gould, E. E. Eyler, W. C. Stwalley, M. Aymar, and O. Dulieu, Eur. Phys. J. D **39**, 261 (2006).